

Molecular binding of Eu(III)/Cm(III) by *Stenotrophomonas bentonitica* and its impact on the safety of future geodisposal of radioactive waste

Ruiz-Fresneda, M. A.; Lopez Fernandez, M.; Martinez-Moreno, M. F.; Cherkouk, A.; Ju-Nam, Y.; Ojeda, J. J.; Moll, H.; Merroun, M. L.;

Originally published:

November 2020

Environmental Science & Technology 54(2020), 15180-15190

DOI: <https://doi.org/10.1021/acs.est.0c02418>

Perma-Link to Publication Repository of HZDR:

<https://www.hzdr.de/publications/Publ-29963>

Release of the secondary publication
on the basis of the German Copyright Law § 38 Section 4.

1 RESEARCH ARTICLE

2

3 **Molecular binding of Eu^{III}/Cm^{III} by *Stenotrophomonas bentonitica* and its impact
4 on the safety of future geodisposal of radioactive waste**

5

6 Miguel A. Ruiz-Fresneda^{1,*}, Margarita Lopez-Fernandez^{1,*#}, Marcos F. Martínez-
7 Moreno¹, Andrea Cherkouk², Yon Ju-Nam³, Jesús J. Ojeda³, Henry Moll², Mohamed L.
8 Merroun¹

9

10 ¹Department of Microbiology, University of Granada, Granada, Spain

11 ²Institute of Resource Ecology, Helmholtz-Zentrum Dresden-Rossendorf e.V., Dresden,
12 Germany

13 ³Systems and Process Engineering Centre, College of Engineering, Swansea University,
14 Swansea, UK

15

16 *Corresponding author/s: Miguel Angel Ruiz-Fresneda. Email: mafres@ugr.es;
17 Margarita Lopez-Fernandez. Email: margaritalopez@ugr.es

18

19 #Present address: Institute of Resource Ecology, Helmholtz-Zentrum Dresden-
20 Rossendorf e.V., Dresden, Germany

21

22

23 **1. Abstract**

24 Microbial communities occurring in reference materials for artificial barriers (*e.g.*
25 bentonites) in future deep geological repositories of radioactive waste can influence the
26 migration behavior of radionuclides such as curium (Cm^{III}). This study investigates the
27 molecular interactions between Cm^{III} and its inactive analogue europium (Eu^{III}) with the
28 indigenous bentonite bacterium *Stenotrophomonas bentonitica* at environmentally
29 relevant concentrations. Potentiometric studies showed a remarkable high concentration
30 of phosphates at the bacterial cell wall compared to other bacteria, revealing the great
31 potential of *S. bentonitica* for metal binding. Infrared spectroscopy (ATR-FTIR) and X-
32 ray photoelectron spectroscopy (XPS) confirmed the role of phosphates and carboxylate
33 groups from the cell envelope in the bioassociation of Eu^{III} . Additionally, time-resolved
34 laser-induced fluorescence spectroscopy (TRLFS) identified phosphoryl and carboxyl
35 groups from bacterial envelopes, among other released complexing agents, to be
36 involved in the Eu^{III} and Cm^{III} coordination. The ability of this bacterium to form a
37 biofilm at the surface of bentonites allow them to immobilize trivalent lanthanide and
38 actinides in the environment.

39

40

41 **Keywords:** europium, curium, bacterial speciation, mobility, geodisposal

42

43

44

45

46

47

48 **2. Introduction**

49 The safe disposal of radioactive waste is crucial to ensure the safety of future
50 generations, as well as for the biosphere. The implementation of deep geological
51 repositories (DGRs) is planned in the near future for the disposal of high level (HLW)
52 and long-lived radioactive wastes, which are the most hazardous since they contain
53 larger radionuclide concentrations and longer lived radionuclides.¹ DGR is a multi-
54 barrier system to deposit radioactive waste, mainly generated by nuclear industry. A
55 DGR option is to encapsulate the nuclear waste in metal containers (steel, iron, copper,
56 etc.) surrounded by compacted bentonites, considered as geotechnical barriers, and
57 emplace them in a stable geological formation at about 500-1000 m depth.² A high
58 microbial diversity in bentonite clay formations from Almeria (Spain), considered as
59 reference material of engineered barriers for repositories, has been previously
60 reported.^{3,4} Several studies have evidenced the impact of microbial processes on the
61 corrosion of metal containers (steel, iron, copper, etc.), which could lead to the release
62 of radionuclides to the surrounding environment.⁵ Microbial processes also seem to play
63 a crucial role controlling the speciation and mobility of radionuclides present in
64 radioactive wastes, such as uranium (U) and curium (Cm).^{3,4,6} Therefore, understanding
65 the migration behavior and the environmental fate of radionuclides influenced by
66 microorganisms will be essential for the risk assessment of repositories. Cm is a highly
67 toxic radionuclide as indicated by the high α activity of some isotopes, such as ²⁴⁷Cm
68 (half-life: 1.6×10^7 years) and ²⁴⁸Cm (half-life: 3.5×10^6 years) present in nuclear spent
69 fuel.^{7,8} Cm is a representative of trivalent actinides (An^{III}), which exhibits excellent
70 luminescence properties that make it suitable for direct speciation studies at
71 environmentally relevant metal concentration.⁹ Similarly, europium (Eu) has been

72 studied as an inactive analogue of An^{III}, also providing excellent luminescence
73 properties.¹⁰

74 Among other mechanisms, microbes can interact with actinides and lanthanides through
75 the biosorption at cell surfaces.¹¹ A number of functional groups (*e.g.* carboxyl,
76 phosphoryl) on microbial surfaces have been described to be effective for actinide
77 complexation.^{12,13} Cm^{III} and Eu^{III} form strong complexes with phosphoryl and carboxyl
78 sites of the bacterial cell wall of *Sporomusa* sp. MT-2.99 and *Pseudomonas*
79 *fluorescens*.^{12,14} Recently, Yeasts and Archaea have also been investigated for their
80 ability to complex An^{III} (*e.g.* Cm) and trivalent lanthanides (Ln^{III}) (*e.g.* Eu) through
81 carboxyl and phosphate groups.^{15,16} In addition, biofilm formation by microorganisms
82 has to be considered, as it could lead to the immobilization of bioabsorbed radionuclides
83 within the DGR system and consequently, could affect their integrity.

84 Since cell surfaces play a major role in the complexation of Cm^{III} and Eu^{III}, different
85 spectroscopic and microscopic techniques can be used to investigate the contribution of
86 functional groups and the corresponding mechanisms involved in the biosorption of
87 these elements. Attenuated total reflection-Fourier transform infrared (ATR-FTIR)
88 spectroscopy, X-ray photoelectron spectroscopy (XPS), and time-resolved laser-induced
89 fluorescence spectroscopy (TRLFS) are useful spectroscopic tools to determine the
90 chemical speciation of these elements at environmentally relevant conditions.
91 Potentiometric titrations have been used to determine types and abundance of active
92 metal binding sites at the cell surface.^{17,18} While a multidisciplinary approach
93 combining different microscopic, spectroscopic, and potentiometric titration based
94 methods is usually applied to investigate the interactions of U, as hexavalent actinide,
95 with microbes,^{13,19} the microbial interactions with Cm and Eu have only covered the use
96 of TRLFS and potentiometric techniques.^{12,14}

97 Spanish bentonite clays (Almeria, Spain) have shown to be excellent and suitable
98 reference material of engineered barriers for DGRs due to their physico-chemical
99 properties (low permeability, plasticity, high swelling pressure, thermal conductivity,
100 etc.).⁴ From these clays, *Stenotrophomonas bentonitica* has been isolated and well
101 characterised,²⁰ and shown to influence the chemical speciation and mobility of other
102 elements present in radioactive waste such as selenite (Se^{IV}) and U^{VI} .^{4,21} However, the
103 interactions between $\text{Eu}^{\text{III}}/\text{Cm}^{\text{III}}$ and *S. bentonitica* have never been described before.
104 For all mentioned above, the use of this strain as a model bentonite bacterial strain to
105 investigate the impact of bentonite microbial population in the speciation of
106 radionuclides within the concept of DGR is novel and could provide interesting results
107 with regard to the biological, chemical and physical analysis that are currently
108 undergoing to evaluate the DGR safety.

109 The present work studies the effect of *S. bentonitica* on the environmental fate of Eu^{III}
110 and Cm^{III} under aerobic and anaerobic conditions, analogous to those expected in the
111 geodisposal of radioactive waste. For this purpose, a combination of spectroscopic
112 (ATR-FTIR, XPS, TRLFS) and microscopic (STEM-HAADF: Scanning Transmission
113 Electron Microscopy-High Angle Annular Dark Field) techniques have been employed.
114 This study will provide new insights on the influence of bentonite bacterial isolates in
115 the immobilization of An^{III} within the concept of radioactive waste disposal, and will be
116 useful to compare with other studies using elements such as Se and U. The safety of the
117 DGR system have been well studied from a geological, chemical, and physical point of
118 view, but not many studies have been conducted on the influence of microbiology.
119 Therefore, this work is crucial to better understand how microbes can affect the safety
120 of the disposal of such residues, which is a major environmental problem nowadays.

121

122 **3. Materials and Methods**

123 Experimental procedures related to preparation of Eu^{III} and Cm^{III} stock solutions,
124 potentiometric titration of cell surfaces of *S. bentonitica* treated with Eu^{III}, Eu^{III}
125 biosorption experiments, TRLFS experimental setup, and STEM-HAADF analysis are
126 provided in the Supporting Information. Due to the hazardous nature and difficult
127 handling of Cm^{III}, proper safety precautions and methodologies were employed in this
128 study.

129

130 **3.1. Bacterial strain and growth conditions**

131 The bacterial strain used was isolated from bentonite clay formations recovered from
132 Almeria (Spain),⁴ and was recently described as a novel species named
133 *Stenotrophomonas bentonitica* BII-R7^T.²² The cells were grown aerobically in Luria-
134 Bertani (LB) broth medium (tryptone 10 g/L, yeast extract 5 g/L and NaCl 10 g/L, pH
135 7.0 ± 0.2) at 28 °C under agitation (180 rpm).

136

137 **3.2. Attenuated total reflection-Fourier transform infrared (ATR-FTIR) spectroscopy**

138 *S. bentonitica* cells were suspended in a 30 µM Eu^{III} chloride solution (EuCl₃·6H₂O)
139 under aerobic conditions at pH 6. After 48 hours, the samples were collected by
140 centrifugation (2700 x g; 10 min) and washed with 0.1 M NaClO₄. Finally the samples
141 were lyophilized according to standard protocols.^{17,23} Bacterial cells without addition of
142 Eu^{III} were employed as controls.

143 ATR-FTIR measurements were performed on a Perkin Elmer Spectrum Two
144 spectrometer, equipped with an ATR accessory, consisting of a diamond crystal at a
145 fixed angle of 45°. 32 scans with spectral resolution 4 cm⁻¹ and wavenumber range from

146 4000 to 400 cm⁻¹ were collected for each sample. All measurements were performed in
147 triplicate.

148

149 3.3. X-ray photoelectron spectroscopy (XPS)

150 Eu^{III}-treated cells of *S. bentonitica* were prepared as described in the section 1.3 of the
151 Supporting Information. The obtained powder was mounted on standard sample studs
152 using double-sided adhesive tape. Non-treated cells were prepared and used as controls.
153 XPS measurements were made on a KRATOS SUPRA Photoelectron Spectrometer at
154 10 KV and 20 mA using a monochromatic Al K α X-ray source (1486.6 eV). The take-
155 off angle was fixed at 90°. On each sample the data were collected from three randomly
156 selected locations, and the area corresponding to each acquisition was 400 μ m in
157 diameter. Each analysis consisted of a wide survey scan (pass energy 160 eV, 1.0 eV
158 step size) and high-resolution scan (pass energy 20 eV, 0.1 eV step size) for component
159 speciation. All experiments were conducted in triplicate. The binding energies of the
160 peaks were determined using the C_{1s} peak at 284.5 eV. The software CasaXPS 2.3.17
161 was used to fit the XPS spectra peaks.²⁴

162

163 3.4. Time-resolved laser-induced fluorescence spectroscopy (TRLFS) analyses

164 TRLFS measurements were performed in order to determine Eu^{III}/Cm^{III} species
165 involved in interactions with the bacterial cells. Cells of *S. bentonitica* were brought
166 into contact with 30 μ M Eu^{III} both aerobically and anaerobically and with 0.3 μ M Cm^{III}
167 anaerobically, and collected as indicated in section 1.3 of the Supporting Information.
168 The inactivity and hence easy handling of Eu^{III} allowed the TRLFS studies under both
169 respiring conditions. The Cm^{III} experiments were performed anaerobically in a glove
170 box in order to exclude carbonate complexation of Cm^{III} and for radiation protection

171 issues. The obtained pellets were washed and subsequently re-suspended in 5 mL of 0.1
172 M NaClO₄ for analysis by TRLFS. For Eu^{III}, the pH was kept constant at 6, while
173 varying the incubation time (1, 24 and 48 h). For Cm^{III}, a pH dependent spectroscopic
174 titration (pH 2.33 to 8.04) was carried out.

175

176 **4. Results and discussion**

177 4.1. Potentiometric titration studies

178 The potentiometric titrations curves of *S. bentonitica* BII-R7 before and after Eu^{III}
179 exposure are presented in Figure S1. The concentration of deprotonated sites is
180 standardized per mass of dry biomass (mol g⁻¹), and calculated according to Fein et al.²⁵
181 To calculate the acidity constants and the total concentration of each binding site, data
182 from the titrations curves were fitted using ProtoFit 2.1 rev1,²⁶ using a Non-
183 Electrostatic Model (NEM). It has been demonstrated that electrostatic treatments, such
184 as diffuse layer and triple layer electrostatic models to titration data, greatly over-predict
185 the effect of ionic strength on bacterial surface protonation reactions, resulting in poorer
186 fits and more variability in stability constants than non-electrostatic models.^{27,28}

187

188 The titrated bacterial suspensions exhibited a protonation-deprotonation behaviour over
189 the whole pH range studied (Figure S1). The shape of the titrations curves obtained
190 suggested the presence of functional groups with close acid-base pK_a values, showing
191 that although some small variability could be perceived in each set of the same bacterial
192 sample, essentially reproducible results were obtained (the variation between the
193 titration curves was below 6% of [H⁺]_{exchanged} between pH 3.5 and 10.0). Although a
194 small hysteresis could be observed between acid and base titrations at the same ionic

195 strength, results from reverse titrations did not vary strongly and suggested a reversible
196 proton adsorption/desorption reaction.

197 Table S1 summarizes the pK_a values for *S. bentonitica* before and after Eu^{III} exposure.
198 The calculated values were 4.97 ± 0.08 and 4.78 ± 0.06 for pK₁, 6.88 ± 0.02 and $6.75 \pm$
199 0.13 for pK₂, and 9.43 ± 0.02 and 9.48 ± 0.11 for pK₃. The obtained pK_a values are
200 representative of carboxylic groups for pK₁, phosphate groups for pK₂ and amine and
201 hydroxyl groups for pK₃.^{17,18,25,29–32}

202 The existence of pH zero proton charge (pH_{zpc}) indicated that *S. bentonitica* developed a
203 positive net charge at low pH values, indicating the presence of at least one positively
204 ionising, plausibly amino group. Models which only include negatively ionising groups
205 such as carboxyl, phosphoryl and hydroxyl groups could not develop a net positive
206 charge at low pH.³³ The pH_{zpc} around 5.7 also indicated that the cells were negatively
207 charged at neutral pH = 7 and electrostatic attraction with positive-charged mineral
208 surfaces or metals is favourable.

209 The surface site densities obtained using ProtoFit are also presented in Table S1. The
210 pK_a values for bacterial samples with and without Eu^{III} were comparable, indicating
211 similar concentration of the active functional groups on the cell wall. One exception
212 was found, the concentrations corresponding to phosphate groups (C₂) was significantly
213 lower for *S. bentonitica* cells exposed to Eu^{III}. This could suggest a strong affinity of
214 Eu^{III} to phosphate sites, making them inaccessible to the protonation/deprotonation
215 reaction. The considerable high concentration of phosphate groups at the surface of *S.*
216 *bentonitica* ($10.78 \pm 0.31 \times 10^{-4}$ mol/g) comparing with other bacterial species such as
217 *Sporomusa* sp. MT-2.99 ($5.30 \pm 0.8 \times 10^{-4}$ mol/g), *Sphingomonas* sp. S15-S1 ($3.16 \pm$
218 0.56×10^{-4} mol/g), or *B. sphaericus* JG-7B ($2.19 \pm 0.25 \times 10^{-4}$ mol/g)^{12,34} (Table S1)
219 pointed out the potentially high metal-binding ability of *S. bentonitica*.

220 The results of potentiometric titration experiments indicated that the cell surface groups
221 capable for metal binding sites could involve carboxyl groups (pK around 3-5),
222 phosphate groups (pK around 6-7), and hydroxyl and amine groups ($pK > 8$). These
223 findings are in agreement with previous studies on bacterial surfaces.^{17,35,36} Liu et al.³⁶
224 demonstrated the role of carboxyl, phosphoryl, and amino functional groups of
225 *Synechococcus* sp. PCC 7002 cells as metal surface ligands by means of potentiometric
226 titrations. In the case of Eu^{III} and Cm^{III}, their sorption on the cell envelope of
227 *Sporomusa* sp. MT-2.99, *B. subtilis* and *P. fluorescens* can be due to their coordination
228 with carboxyl and phosphate groups.^{12,14,37,38} Consequently, phosphate and carboxyl
229 groups of *S. bentonitica* might be expected to be involved in the binding of Eu^{III}.
230 However, the potentiometric results only showed phosphate groups as the main
231 potential binding sites in the pH range studied due to their high surface concentration. It
232 is probable that the extent of the carboxyl group involvement in the Eu^{III} binding is
233 either too small to be detected by titration methods, or the sorption/desorption of Eu^{III}
234 by the carboxylic groups is reversible at low pH (possible exchange between Eu(III) and
235 protons at low pH for the carboxylate groups).

236

237 4.2. Eu^{III} removal capacity of *S. bentonitica* over time

238 These studies were carried out to estimate the Eu^{III} removal capacity of *S. bentonitica*
239 with increasing time under aerobic and anaerobic conditions. The maximum amount of
240 Eu^{III} removal was 12.9 ± 0.11 mg of Eu/g of dry biomass after 96 h of aerobic
241 incubation (Figure S2). This amount corresponds to a $54 \pm 0.44\%$ of Eu^{III} removed
242 from the total amount of Eu in the solution. Higher values were obtained by Bader et al.
243 (2019)¹⁶ in their bioassociation kinetics studies with the halophilic archaeon
244 *Halobacterium noricense* DSM15987^T by using the same Eu^{III} initial concentration (30

245 μM). They found that around 73% of Eu^{III} was removed after 1 week of incubation.
246 Under anaerobic conditions, the maximum amount of Eu^{III} removal was 6.06 ± 0.25 mg
247 of Eu/g of dry biomass after 18 h incubation (Figure S2), which corresponds to a $31.2 \pm$
248 1.3 % of Eu^{III} removal. The Eu^{III} removal improved by increasing contact time of
249 incubation until equilibrium was attained under both conditions. However, these results
250 clearly showed that *S. bentonitica* cells have a higher removal capacity under aerobic
251 conditions. This could be a consequence of the more stressful anoxic conditions,
252 probably affecting the bacterial interaction process.

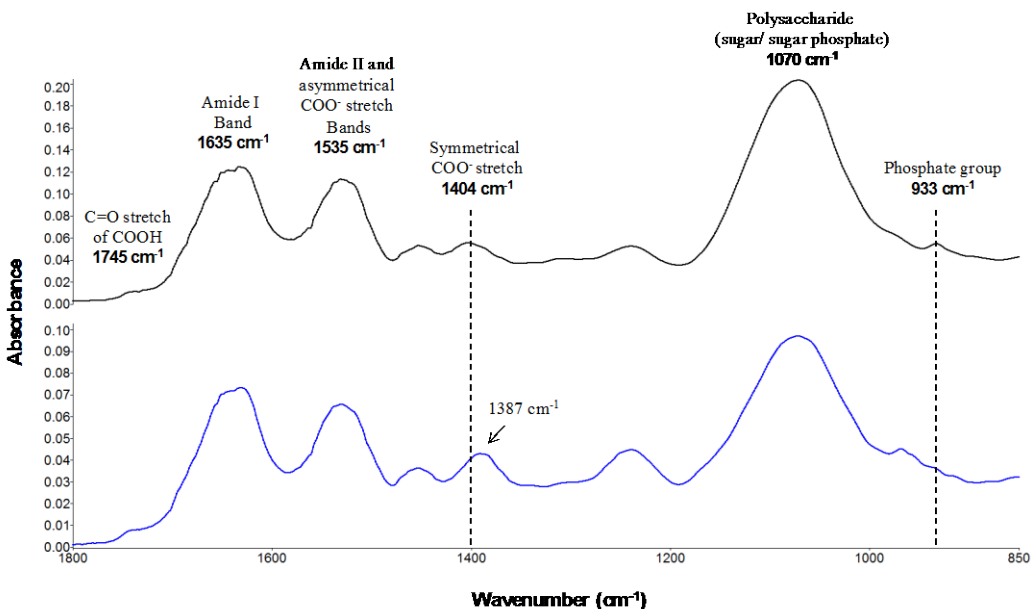
253 These results suggested that the interaction was mediated not only by biosorption, since
254 this mechanism is generally defined as a quick process occurring up to a few hours.³⁹
255 More specifically, the Eu^{III} removal studies showed that time-dependent Eu interaction
256 with the cells could be a biphasic process. First, a rapid phase where 12.5 ± 0.73 and
257 13.9 ± 1 % of Eu^{III} removal was achieved (aerobically and anaerobically, respectively)
258 within the first 2 h (Figure S2). This fast phase is usually associated to metabolic
259 independent biosorption mechanisms. Secondly, a slow phase seems to occur, where
260 Eu^{III} accumulation process seems to reach equilibrium after 24 h. This phase could be
261 controled by metabolically dependent interaction mechanisms such as intracellular
262 accumulation or bioprecipitation, among others.

263

264 4.3. Characterization of Eu^{III}-*S. bentonitica* interactions using ATR-FTIR

265 Figure 1 shows the ATR-FTIR spectra obtained from *S. bentonitica* after 48 h
266 incubation with 30 μM Eu^{III} solution. The observed infrared bands confirmed the
267 presence of proteins, lipids, polysaccharides, and polyphosphate groups. The functional
268 groups assigned to the infrared bands and the corresponding frequencies for the
269 bacterial cells are summarised in Table S2.

270 The region between 3000 and 2800 cm⁻¹ exhibited the typical C-H stretching vibrations
271 (ν_{C-H}) corresponding to the CH₃ and >CH₂ functional groups present in the fatty acids
272 and lipids, and the O-H stretching band (ν_{O-H}) corresponding to the presence of
273 hydroxyl groups in bacterial cells. Complementary information could be found at the
274 region between 1800 and 750 cm⁻¹, where vibrations of C-H, >CH₂ and -CH₃ groups,
275 amides, carbonyl groups and polysaccharides were observed. The peaks observed at
276 1308 and 1455 cm⁻¹ could be attributed to the bending of -CH₃ and >CH₂ of proteins
277 (δ_{CH_2} , δ_{CH_3}), and the signals at 1635 and 1535 cm⁻¹ corresponded to the amide I and II
278 bands, respectively. The amide I band was due to the stretching C=O ($\nu_{C=O}$) of amides
279 associated with proteins and the amide II band was actually a combination of bending
280 N-H (δ_{N-H}) of amides and contributions from stretching C-N (ν_{C-N}) groups. The peak at
281 1455 cm⁻¹ also concealed the amine III group. The peak around 1404 cm⁻¹ was due to
282 the symmetric stretching C-O of carboxylate groups ($\nu_{sym\ coo^-}$), and the peak
283 corresponding to the asymmetric stretching vibration ($\nu_{asym\ coo^-}$) was concealed by the
284 amide II band at 1535 cm⁻¹. A small shoulder around 1745 cm⁻¹ was a combination of
285 two peaks: a signal corresponding to the vibrational C=O stretching ($\nu_{C=O}$) of carboxylic
286 acids at 1747 cm⁻¹ and another peak corresponding to the stretching C=O of ester
287 functional groups from membrane lipids and fatty acids at 1730 cm⁻¹.^{17,30,31,40} The
288 double bond stretching of >P=O of general phosphoryl groups and phosphodiester of
289 nucleic acids could be observed at 1240 cm⁻¹. The stretching of P=O groups of
290 polyphosphate products, nucleic acid phosphodiester and phosphorylated proteins can
291 be found around 1070 cm⁻¹, and the peak at 933 cm⁻¹ showed the asymmetric O-P-O
292 stretching modes.^{30,31,40}



293

294 **Figure 1.** Comparison between the ATR-FTIR spectra for *S. bentonitica* cell
295 suspensions in 0.1 M NaClO₄ (electrolyte) solution only (top, in black color) and in 30
296 μM Eu^{III} solution + electrolyte (bottom, in blue color) after 48 hours.

297

298 The ATR-FTIR spectra showed a shift in the band attributed to symmetric stretching of
299 carboxylate groups (around 1404 cm⁻¹) to lower frequencies, when compared to the
300 spectra of the cells in background electrolyte (Figure 1). Extensive studies made on
301 metal complexes of carboxylic acids have established an empirical correlation between
302 the position of the symmetric stretching ($\nu_{\text{sym}} \text{COO}^-$) and asymmetric stretching ($\nu_{\text{asym}} \text{COO}^-$)
303 of carboxylate groups and the difference in frequency between them ($\Delta\nu$). The values of
304 $\Delta\nu$ descend in the follow order: $\Delta\nu_{\text{unidentate}} > \Delta\nu_{\text{brinding}} \sim \Delta\nu_{\text{free ionic}} > \Delta\nu_{\text{chelate(bidentate)}}$.⁴¹⁻⁴⁴

305 Chu et al.⁴¹ and Deacon and Phillips,⁴⁴ after careful examinations of IR spectra of many
306 acetates with known X-ray crystal structures, arrived at the conclusion that: i) for
307 unidentates complexes, $\Delta\nu > 200 \text{ cm}^{-1}$ and the position of $\nu_{\text{sym}} \text{COO}^-$ is generally shifted
308 to lower frequencies; ii) for bidentate chelating complexes, $\Delta\nu < 100 \text{ cm}^{-1}$ and the
309 position of $\nu_{\text{sym}} \text{COO}^-$ is shifted to higher frequencies, whereas $\nu_{\text{asym}} \text{COO}^-$ is shifted to

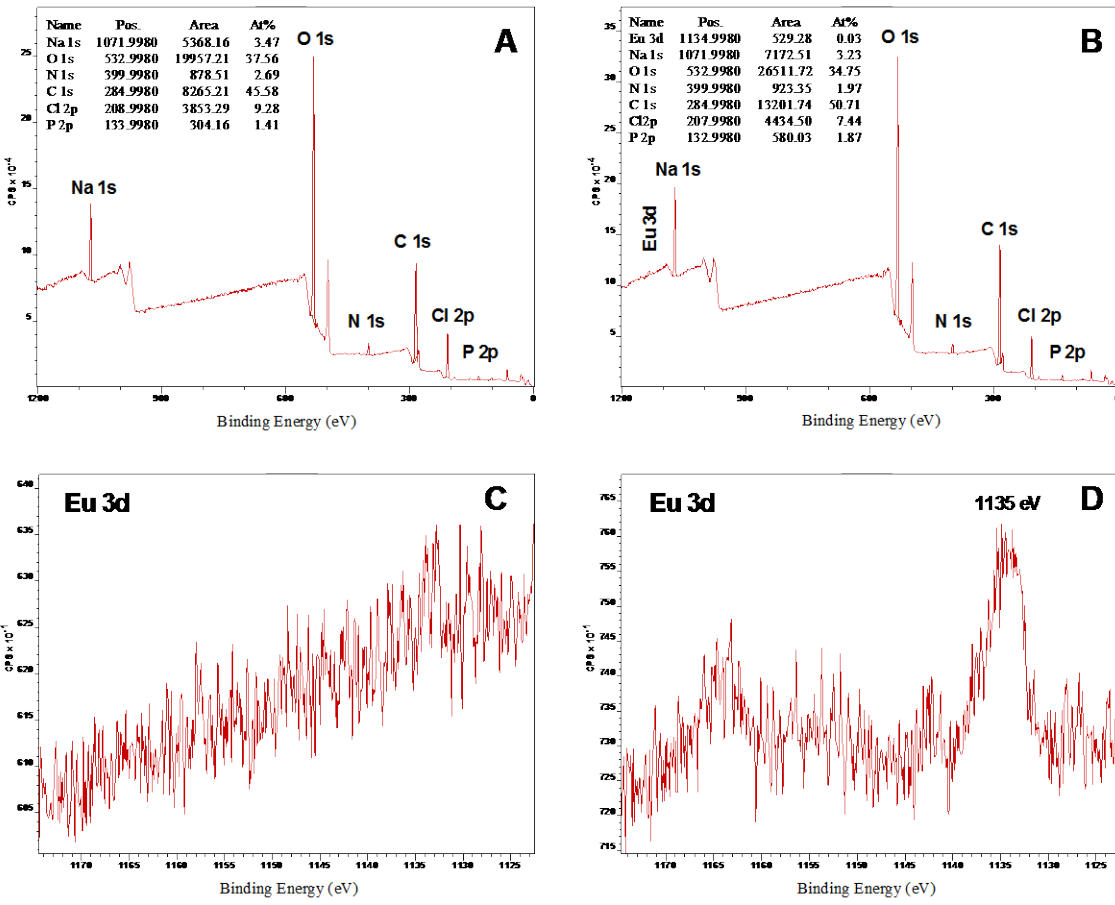
lower frequencies; and iii) for bidentate bridging complexes, $\Delta\nu \sim 160\text{ cm}^{-1}$ and the position of $\nu_{\text{sym}}\text{ COO}^-$ and $\nu_{\text{asym}}\text{ COO}^-$ can shift in either direction.⁴¹ The symmetric stretching ($\nu_{\text{sym}}\text{ COO}^-$) band for *S. bentonitica* in contact with Eu^{III} shifted to lower frequencies by $\sim 15\text{ cm}^{-1}$, but, as can be observed in Figure 1 and Table S2, the asymmetric stretching ($\nu_{\text{asym}}\text{ COO}^-$) of carboxylate groups was hidden by the amide II band, and therefore it is difficult to determine if there was a shift in this band to higher or lower frequencies. Based purely on the position of $\nu_{\text{sym}}\text{ COO}^-$ shifting to lower frequencies, the carboxyl functional groups could form unidentate complexes with the Eu^{III} metals. If the asymmetric stretching ($\nu_{\text{asym}}\text{ COO}^-$) of carboxylate groups (hidden by the amide II band) did not shift, then $\Delta\nu$ would be around 150 cm^{-1} , suggesting that the carboxyl functional groups arising from the macromolecules of the cell wall of the bacterial cells could form bidentate bridging complexes with the Eu^{III} metals. However, further studies would be needed as there is no evidence of the frequency of the asymmetric $\nu(\text{COO}^-)$ mode. EXAFS analysis could provide more detailed information about the local coordination of Eu associated with these cells, but it falls beyond the main scope of this study. This would provide more unequivocal indications of the ability of bentonite-isolated bacteria to interact with Eu in a unidentate or bidentate bridging mode. Nevertheless, these results provide further verification that carboxyl functional groups from the macromolecules of the bacterial cells are responsible in forming organo-metallic complexes with the Eu^{III} metals, as also reported by the potentiometric and luminiscence results.

In addition, the ATR-FTIR spectra indicated that phospholipids might also be involved in the cell-metal complexation. The lower intensity of the band found at 933 cm^{-1} of Eu^{III}-treated cells compare with Eu^{III}-untreated cells suggests phosphate groups as candidates for Eu^{III} complexation.²³

335 4.4. Characterization of Eu^{III}-*S. bentonitica* interactions using XPS.

336 This method was applied to determine the local coordination of Eu^{III} at the cell surface
337 of *S. bentonitica* approximately up to 5 nm.⁴⁵ The elemental composition of the *S.*
338 *bentonitica* surface, resulting from integrating the C_{1s}, O_{1s}, N_{1s} and P_{2p} from the wide
339 scan spectrum can be seen in Figure 2A-D. Sodium and chlorine were also detected as
340 samples were washed with 0.1 M NaClO₄. Eu was detected in the bacterial sample in
341 contact with a 30 μM Eu^{III} solution for 48 hours. Nitrogen appeared at a binding energy
342 of 399.99 eV, attributable to amine or amide groups of proteins.^{23,46-49} Phosphorus was
343 found at a binding energy of 133.99 eV, and can be attributed to phosphate groups.⁴⁷⁻⁴⁹
344 The presence of amine groups from proteins and phosphate groups based on the binding
345 energies of N_{1s} and P_{2p} are in agreement with the results from potentiometric titrations
346 (pK_a = 6.8 and pK_a = 9.4) and the FTIR spectra (adsorption bands at 1635 cm⁻¹, 1535
347 cm⁻¹, and 933 cm⁻¹).

348 XPS peaks corresponding to Eu_{3d} were also analysed at high resolution to assess the
349 nature of the Eu^{III} complex and shown in Figure 2D. The local coordination of Eu
350 associated to the cells of the studied strain, observed at 1135 eV, is similar to that of Eu-
351 acetate as was described by Mercier et al.⁵⁰ This suggests that carboxyl groups
352 containing cell wall molecules like glutamic acid of peptidoglycan are involved in the
353 Eu binding. Previous studies showed the role of carboxyl groups from glutamic and
354 aspartic acid present in proteins of the S-layer of *B. sphaericus* in the complexation of
355 uranium and palladium.^{51,52} Therefore, carboxyl groups of the glutamic acid of the
356 peptidoglycan (PG) layer of *S. bentonitica* could be involved in the interaction of Eu^{III}.



357

358 **Figure 2.** XPS spectra of *S. bentonitica* in absence (A, C) and presence of 30 μM Eu^{III}
359 (B, D). High-resolution spectra of the region belonging to Eu 3d (C and D).

360

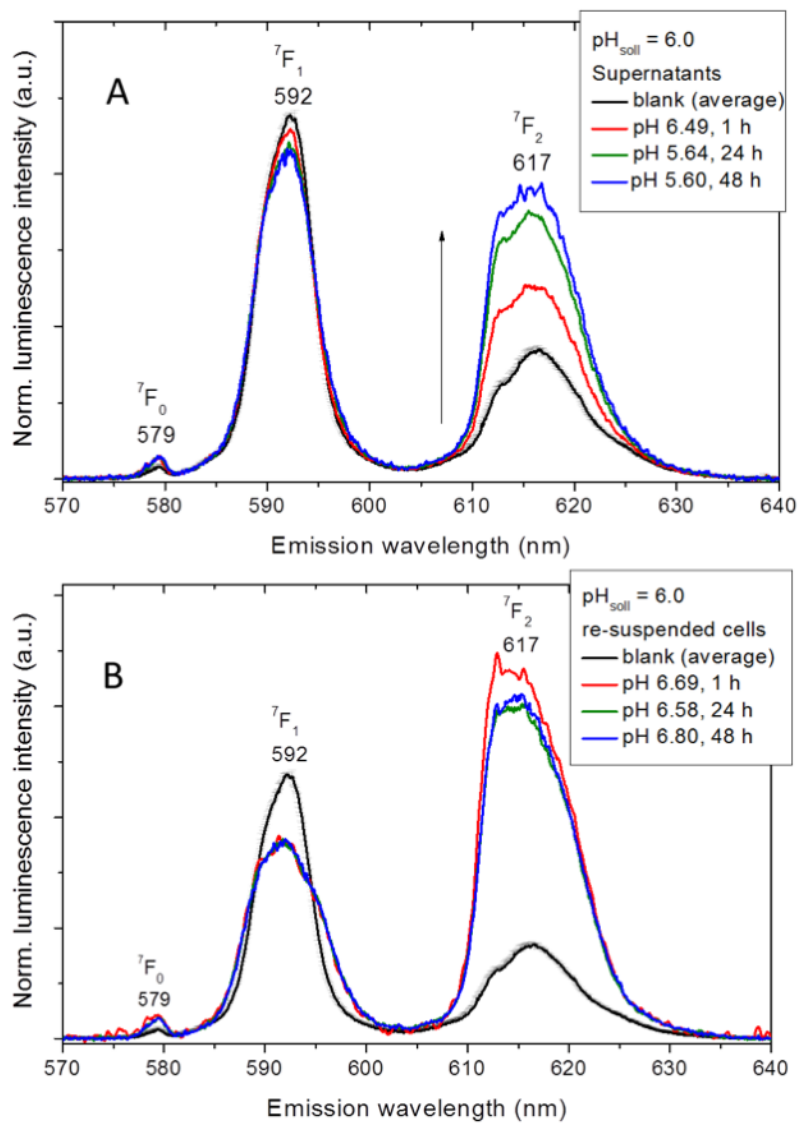
361 4.5. TRLFS characterization of Eu^{III}/Cm^{III} interaction with *S. bentonitica*
362 Potentiometric titrations, ATR-FTIR, and XPS studies showed the involvement of
363 phosphate and carboxyl groups in the coordination of Eu^{III} by the *S. bentonitica* cells. In
364 addition, Eu^{III} and Cm^{III} were used as luminescence probes to investigate Cm^{III}/Eu^{III}
365 binding on *S. bentonitica* based on changes of the intrinsic luminescence properties due
366 to microbial interaction. The studies with Cm^{III}, radioactive analogue of Eu^{III}, were
367 carried out at much lower concentrations relevant to environmental conditions (0.3
368 μM).
369

370 4.5.1. *Europium*

371 The luminescence spectra depicted in Figure 3 showed the interaction of Eu^{III} with *S.*
372 *bentonitica* through typical changes as result of cell addition after 1, 24 and 48 h of
373 anaerobic incubation at pH 6 in both, supernatants and re-suspended cells. This
374 suggested the complexation of Eu^{III} with extracellular released complexing agents and
375 bacterial surface functional groups, respectively. In the supernatant and the re-
376 suspended cells the ⁷F₀ transition appeared at 579 nm with a slightly higher intensity
377 than in the blank sample. This pointed to a different symmetry around the Eu^{III} center
378 compared to the blank spectrum and is a further argument for interaction process of
379 Eu^{III} with the cells. The luminescence spectrum of Eu^{III} aqua ion (blank) is
380 characterized by emission bands at 585-600 nm (magnetic dipole transition ⁵D₀ → ⁷F₁)
381 and 610-630 nm (hypersensitive transition ⁵D₀ → ⁷F₂). An increased intensity of the
382 hypersensitive ⁷F₂ transition at 617 nm moving from blank via supernatant to the re-
383 suspended cells was discovered.

384 In the supernatants, there was a systematic increase in the ⁷F₂ transition as a function of
385 the incubation time (Figure 3A). This could indicate an increase in the release of
386 complexing agents from the cells at a longer incubation time. Total organic carbon
387 (TOC) content of the supernatant samples increased after 24 h of incubation (Figure
388 S3), suggesting the release of complexing substances from the cells. These results are in
389 agreement with the Eu^{III} removal studies (section 4.2), in which the amount of Eu
390 adsorbed increased with the incubation time. In the re-suspended cells, there was a fast
391 rise in the intensity of the ⁷F₂ transition after an incubation time of 1 h. Then, no
392 systematic changes in the spectra, as a function of the incubation time, were observed
393 (Figure 3B).

394



395

396 **Figure 3.** Luminescence emission spectra of 30 μ M Eu^{III} measured for the supernatants
 397 after separating the *S. bentonitica* cells (0.2 g/L) (A) and the re-suspended cells (B)
 398 under anaerobic conditions at pH 6 and different incubation times (1, 24 and 48 hours)
 399 in 1 M NaClO₄.

400

401 In supernatants and re-suspended cells, Eu^{III} appeared in two different coordination
 402 environments. The short-lived component in supernatants was measured at 117, 129 and
 403 133 μ s after 1, 24, and 48 h, respectively (Table 1). These lifetimes indicated a similar

404 coordination environment after 24 and 48 h. Those Eu^{III}-species containing
405 approximately eight water molecules and one binding site will be filled by
406 functionalities of the released substances. The luminescence lifetime of $114 \pm 5 \mu\text{s}$
407 corresponding to 8.8 ± 0.5 coordinated water molecules found in the blank was
408 characteristic to the Eu³⁺ ion. The short lifetime of $117 \mu\text{s}$ found in the supernatant after
409 1 h of incubation indicated the presence of the Eu^{III} ion. The longer lifetimes, 387 to
410 $500 \mu\text{s}$, could indicate an interaction of Eu^{III} with released substances from the cells
411 independently from the incubation time. In this second type of Eu^{III} complex only up to
412 1 to 2 water molecules remained. In the case of re-suspended cells, a bi-exponential
413 luminescence decay was measured indicating two coordination environments of Eu^{III}.
414 The short-lived component showed luminescence lifetimes between 144 and $225 \mu\text{s}$ (7
415 and 4 coordinated water molecules, respectively), whereas the long-lived component
416 varied between 477 and $609 \mu\text{s}$ (2 and 1 coordinated water molecules, respectively). In
417 a first approximation, similar Eu^{III} species were formed for the short-lived component of
418 the supernatant and re-suspended cells. In the same way, the long-lived component of
419 both supernatant and re-suspended cells suggested a similar coordination environment
420 but different from the one found for the short-lived component.

421 By comparing our lifetime results with literature data, phosphoryl and carboxyl groups
422 present on bacterial cell envelopes and bacterial released substances seem to play an
423 important role in the Eu^{III} coordination sites characterized by, for instance, their
424 individual luminescence lifetimes, probably in form of R-O-PO₃-Eu²⁺ (R-O-PO₃H-Eu²⁺
425 under acidic pH conditions) and R-COO-Eu²⁺ as revealed by previous studies (Table
426 1).^{12,53} Specifically, the Eu^{III}-*S. bentonitica* complexes seem to have similar properties
427 as the surface species R-O-PO₃H-Eu²⁺ observed on cell envelopes of *Sporomusa* sp.
428 MT-2.99 as revealed by the long lifetimes.¹² The coordination site characterized by

429 short lifetimes seem to interact with Eu^{III} with similar properties as the surface species
 430 R-COO-Eu²⁺ observed on cell envelopes of *Sporomusa* sp. MT-2.99 and *P.*
 431 *fluorescence*.¹² It is important to note that the results presented here were very similar to
 432 those obtained aerobically and have comparable significance (Figure S4).

433

434 **Table 1.** Spectroscopic properties obtained from the Eu^{III}-*S. bentonitica* system at pH 6
 435 using different incubation times and other relevant model systems.

Sample	R _{E/M}	Lifetime (μs)	Proposed species	Reference
Eu^{III} control	0.50	± 114 ± 5	Eu ³⁺	This work
	0.05			
Supernatants				This work
Eu^{III}-<i>S. bentonitica</i>				
1 h incubation	0.9	117; 387	Eu ³⁺ ; phosphoryl sites	
24 h incubation	1.2	129; 490	Carboxyl; phosphoryl	
48 h incubation	1.3	133; 500	Carboxyl; phosphoryl	
Cells				This work
Eu^{III}-<i>S. bentonitica</i>				

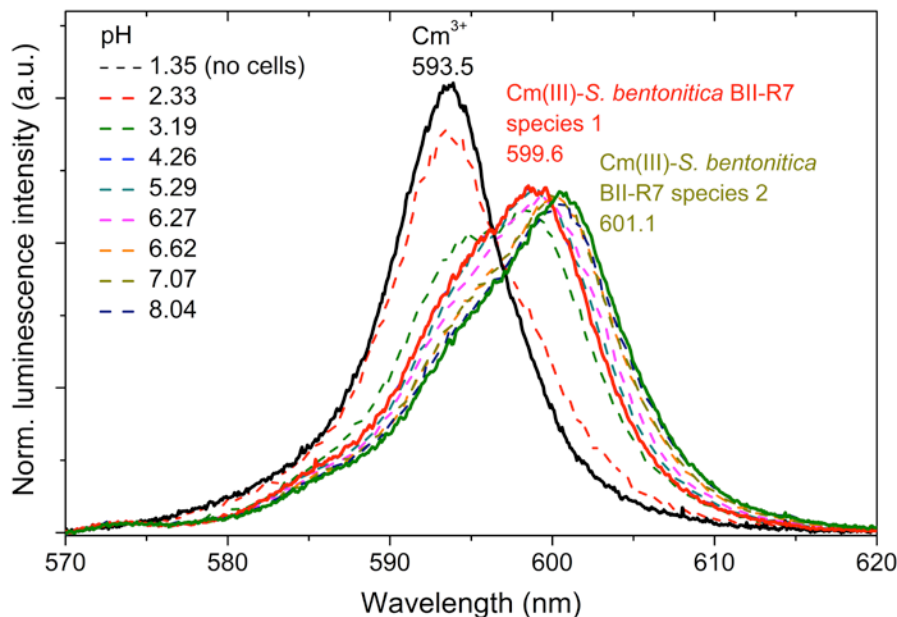
1 h incubation	2.3	144; 477	Carboxyl; phosphoryl sites	
24 h incubation	2.1	174; 561	Carboxyl; phosphoryl	
48 h incubation	2.1	225; 609	Carboxyl; phosphoryl	
Eu^{III}-Sporomusa sp.	3.3	170	R-COO-Eu ²⁺	Moll et al. ¹²
MT-2.99				
	1.8	515	R-O-PO ₃ H-Eu ²⁺	
Eu^{III}-Bacillus subtilis		230	Carboxyl sites	Markai et al. ⁵⁴
		730	Phosphoryl sites	
Eu^{III}-Pseudomonas aeruginosa		98-254	Carboxyl sites	Texier et al. ⁵³
		534-677	Phosphoryl sites	

436

437 4.5.2. Curium

438 The chemical speciation of Cm^{III} with *S. bentonitica* cells was studied at trace (0.3 μM)
 439 Cm^{III} concentrations by TRLFS. These measurements were conducted assuming that the
 440 influence of the luminescence properties of the microbial Cm^{III}-species dominates over
 441 the influence of soluble Cm^{III}-species with, for instance, released complexing agents.

442 The pH-dependent spectroscopic Cm^{III} speciation in the cell suspensions is shown in
443 Figure 4.



444

445 **Figure 4.** Luminescence emission spectra of $0.3 \mu\text{M}$ Cm^{III} in 0.1M NaClO_4 measured as
446 a function of pH at a fixed biomass concentration of $0.2 \text{ g}_{\text{dry weight/L}}$.

447

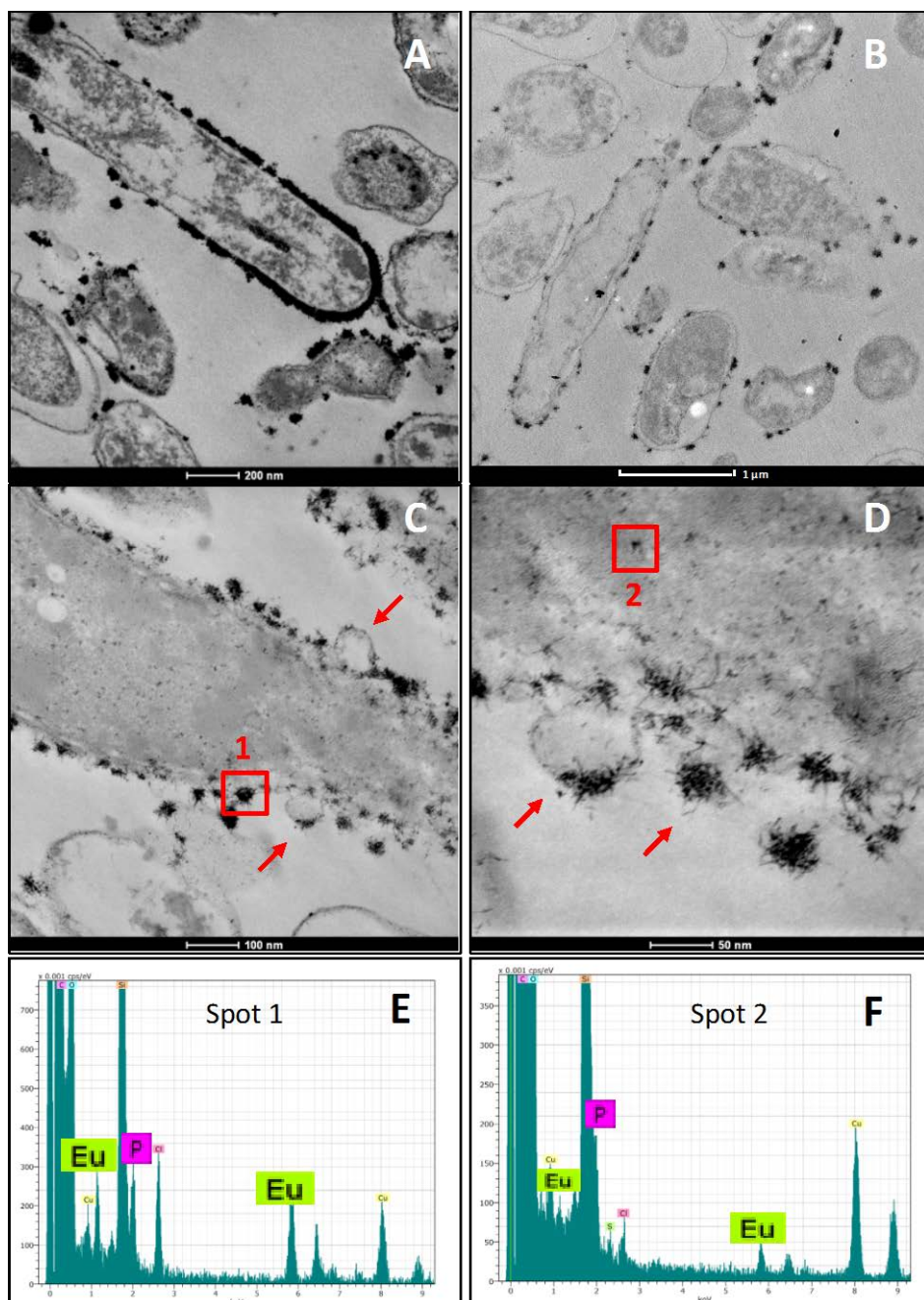
448 From the dependencies found in the TRLFS spectra, it can be concluded that there are
449 two coordination environments of Cm^{III} due to interactions with functional groups of
450 the cell surface and possibly with released complexing agents. Thus, the Hypspec
451 analysis of the pH dependent emission spectra measurements revealed two Cm^{III}
452 bacterial species (Figure 4). $\text{Cm}^{III}\text{-}S. bentonitica$ species 1 was characterized by an
453 emission maximum at 599.6 nm while $\text{Cm}^{III}\text{-}S. bentonitica$ species 2 showed a more red
454 shifted emission maximum at 601.1 nm. The extracted single component spectra of both
455 species are shown in Figure 4. TRLFS of the supernatants and the Cm^{III} loaded biomass
456 after washing with 0.1M NaClO_4 showed that 73% of the detected Cm^{III} luminescence
457 intensity remained in solution at pH 8.04, while, only 23% was associated to the
458 biomass. This evidence indicated that a complexation of Cm^{III} by substances released

459 from the cells was occurring. In all samples containing cells, a bi-exponential
460 luminescence decay was detected (Table S3). At pH 3.2 the short lifetime of 71 μ s
461 points to uncomplexed Cm³⁺. Between pH 4 and 8 both lifetimes amounted to 120 ± 8
462 and 290 ± 23 μ s corresponding to 5 and 2 coordinated water molecules, respectively. By
463 comparing our results with the ones reported in literature, a close agreement was found
464 to the study of Lopez-Fernandez et al.¹⁵ The long lifetime and the corresponding
465 emission maximum matches with Cm^{III} interactions with microbial phosphoryl sites,
466 whereas the short lifetime can be attributed to carboxyl interactions of Cm^{III}.

467

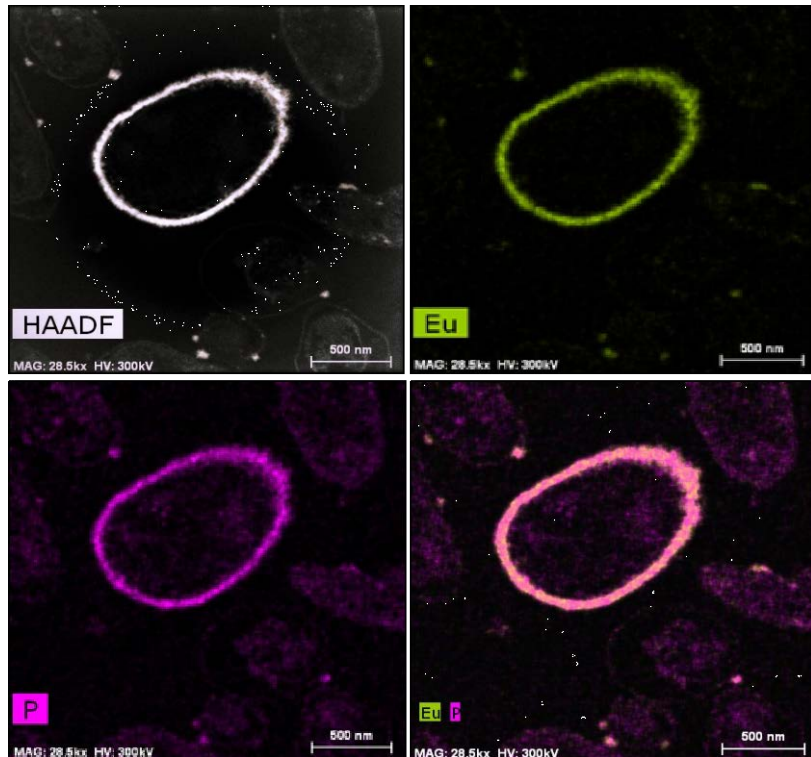
468 4.6. Cellular localization of Eu^{III} by STEM-HAADF (Scanning Transmission Electron
469 Microscopy-High Angle Annular Dark Field).

470 STEM-HAADF micrographs of thin sections of *S. bentonitica* cells exposed to Eu^{III}
471 revealed the presence of electron-dense accumulations, mainly at the cell surface
472 (Figure 5A-D) under both aerobic and anaerobic conditions. In addition, very few
473 extracellular (Figure 5A-D) and intracellular (Figure 5D) accumulations were observed.
474 EDX analysis (Figure 5E-F) and element-distribution mapping (Figure 6) of these
475 accumulations indicated a main composition of Eu and P. The detection of P in the
476 EDX analysis of the Eu^{III} precipitates also confirmed the key role of functional groups
477 containing phosphorus in their interaction with Eu^{III}. These results showed biosorption
478 of Eu^{III} as the main interaction mechanism with the cells of *S. bentonitica*. However, the
479 presence of few extracellular and intracellular Eu^{III} precipitates indicated that the
480 interaction is not only mediated by biosorption, thus other processes, such as
481 bioaccumulation and bioprecipitation, could also occur. This matches very well with the
482 Eu^{III} removal studies (section 4.2.) suggesting the implication of other interaction
483 mechanisms.



486 **Figure 5.** STEM-HAADF micrographs showing electron-dense accumulations at the
 487 cell surface, extracellular, and intracellularly under aerobic (A-B) and anaerobic
 488 conditions (C-D). EDX analysis (E-F) confirming the Eu and P composition of the
 489 accumulations. The formation of vesicles by *S. bentonitica* cells is indicated by arrows
 490 (C-D). Scale bars: 200 nm (A), 1μm (B), 100 nm (C), 50 nm (D).

492 The formation of outer membrane vesicles (OMVs) by *S. bentonitica* cells exposed to
493 Eu^{III} was observed in the STEM-HAADF micrographs (Figure 5C-D). The production
494 of OMVs by Gram-negative bacteria plays a prominent role in cell protection against
495 hostile environments.^{55,56} Moreover, it represents a mechanism to alleviate stress through
496 the packaging and release of stress-products.⁵⁷ Therefore, the vesicle formation
497 mechanism of *S. bentonitica* cells could be involved in their Eu^{III} tolerance. In addition,
498 the detection of extracellular precipitates could be a consequence of the release of
499 intracellular accumulates through the formation of vesicles. However, further
500 investigations are needed to confirm this hypothesis. On the other side, intracellular
501 accumulation could be a consequence of a passive process associated to damage of the
502 cell membrane permeability, since Eu do not play any biological function and the cells
503 do not have a specific transport system for the uptake of this element. The explanation
504 of how and why elements such as Eu are accumulated in the cytoplasm of some
505 microorganisms remains unknown.



506 **Figure 6.** STEM-HAADF micrographs of thin sections showing the adsorption of Eu^{III}
507 on a *S. bentonitica* cell after 48 h in contact with 30 μM Eu^{III} solution. Scale bars: 500
508 nm.
509
510

511 4.7. Environmental implications.

512 The safety of the DGR system have been well studied from a geological, chemical, and
513 physical point of view but, very few works have investigated the impact of microbial
514 processes in the safety of this disposal option. It is well known that microbe occurring
515 in different DGR barriers, including bentonites, could affect the safety of a DGR
516 through: 1) corrosion of metal containers, 2) transformation and alteration of bentonite
517 minerals, 3) gas production, and 4) mobilization of radionuclides present in the system,
518 such as curium, selenium, or uranium. Here we reported a clear effect of the activity of
519 the bentonite bacterial isolate *S. bentonitica*, on the speciation and mobility of trivalent
520 actinides such as Cm^{III} and its inactive analogue Eu^{III}.

521 A multidisciplinary approach combining microscopy, spectroscopy, and potentiometric
522 titration based methods allowed us to provide new insights on the speciation of Cm and
523 Eu associated with bacterial strains (isolated from one of the most important arificial
524 barriers, bentonites, of future DGR). The results obtained revealed that carboxyl and
525 phosphoryl groups from bacterial envelopes and other extracellularly released
526 complexing agents seem to be involved in the interaction with Eu and Cm. Specifically,
527 XPS analysis suggested that these carboxyl groups could arise from macromolecules
528 located at the cell surface such as glutamic acids of the peptidoglycan layer, which
529 could be involved in the complexation of Eu^{III}. In addition, ATR-FTIR suggested that
530 the coordination of Eu^{III} with carboxyl groups from the bacterial cell wall could occur in
531 a bidentate bridging mode. Finally, TEM analysis, in combination with the rest of the
532 techniques, suggested that the Eu/Cm-bacteria interaction most probably occur through
533 several microbial processes such as biosorption, intracellular accumulation, and
534 biomineralization. The results here reported clearly suggested that *S. bentonitica* could
535 influence the speciation and hence mobility of Eu and Cm, affecting the safety of the
536 DGR system.

537

538 Biosorption and bioaccumulation may enable the metal removal from contaminated
539 aqueous solutions through the immobilization of bacterial biomass to inert supports,⁵⁸
540 which are nowadays receiving attention for bioremediation purposes. The
541 immobilization of microorganisms in minerals from bentonites and other materials
542 through the formation of biofilms could lead to the immobilization of bioadsorbed or
543 bioaccumulated radionuclides. Indeed, genes coding for the formation of biofilms such
544 as those involved in the formation of surface structures (*fliA*, *fliB*, *fliR*, *fliQ*, *fliP*, *fliN*,
545 *fliM*)⁵⁹ or those encoding outer-membrane lipoproteins (*slp*)⁶⁰ have been reported to be

546 present in the genome of *S. bentonitica*⁶¹ (GenBank accession number
547 MKCZ00000000). In addition, the production of flagella-like proteins by this bacterium
548 could be involved in the formation of biofilms. Clark et al.⁶² demonstrated the role of
549 flagella-like filaments produced by *Desulfovibrio vulgaris* in the establishment and
550 maintenance of biofilms between cells and silica oxide surfaces. Therefore, *S.*
551 *bentonitica* could positively influence the safety of repositories by inducing the
552 immobilization of radionuclides through the biofilm formation.

553 In addition to biosorption and bioaccumulation, a long-term bioprecipitation process
554 could be involved as suggested by the extracellular Eu precipitates observed by STEM-
555 HAADF. Bioprecipitation basically leads to the immobilization of radionuclides since it
556 is based on the conversion from soluble to insoluble forms through their precipitation
557 with released cell ligands (carbonates, phosphates, etc.).^{11,63} From all mentioned above,
558 the present study could be really helpful to better understand how microbes affect the
559 safety of the disposal of radioactive residues, which is a global environmental concern
560 nowadays.

561

562 **5. Conflicts of interest**

563 The authors declare no competing financial interest.

564

565 **6. Acknowledgements**

566 This work was supported by Euratom research and training programme 2014-2018
567 under grant agreement no. 661880 and ERDF -financed Grants CGL-2012-36505,
568 CGL2014-59616-R (80% finding by FEDER). Part of this work was co-financed by the
569 European Radioecology Alliance mobility grant awarded to MAR-F. The authors
570 acknowledge the assistance of Maria del Mar Abad Ortega and Concepción Hernández

571 Castillo (Centro de Instrumentación Científica, University of Granada, Spain) for their
572 help with microscopy measurements, and Dr James McGettrick (Swansea University,
573 College of Engineering) for the help with the XPS measurements. The authors are
574 indebted to the U.S. Department of Energy, Office of Basic Energy Sciences, for the use
575 of ^{248}Cm via the transplutonium element production facilities at Oak Ridge National
576 Laboratory; ^{248}Cm was made available as part of collaboration between HZDR and the
577 Lawrence Berkeley National Laboratory (LBNL).

578

579 **7. Supporting information**

580 The supporting information includes 5 sections of methodology, 4 figures and 3 tables
581 in a separate file.

582 1. Supplementary materials and methods

583 1.1. Preparation of Eu^{III} and Cm^{III} stock solutions

584 1.2. Potentiometric titration of cell surfaces of *S. bentonitica* treated with Eu^{III}

585 1.3. Eu^{III} biosorption experiments

586 1.4. TRLFS experimental setup

587 1.5. STEM-HAADF analysis

588 2. Supplementary figures and tables

589 Figure S1. Representation of the potentiometric titrations of *S. bentonitica* in 0.1 M
590 NaClO₄ suspension (A) and in contact with 30 μM Eu^{III} solution (B) after 48 hours of
591 incubation, compared with the background electrolyte. Closed symbols correspond to
592 the forward titration data and open symbols correspond to back titration.

593 Figure S2. Time dependence in the Eu^{III} removal capacity of *S. bentonitica* cells under
594 aerobic (A and B) and anaerobic (C and D) conditions. The Eu^{III} removal is expressed
595 as mg of Eu per g of dry biomass (A and B) and percentage (B and D).

596 Figure S3. Total organic carbon as a function of time of supernatants obtained after
597 Eu^{III}-*S. bentonitica* interaction under anaerobic conditions.

598 Figure S4. Luminescence emission spectra of 30 μM Eu^{III} measured for the supernatants
599 after separating the *S. bentonitica* cells (0.2 g/L) and the re-suspended cells under
600 aerobic conditions at pH 6 and 24 h incubation in 1 M NaClO₄ (A). Spectroscopic
601 properties obtained from the Eu^{III}-*S. bentonitica* system (B).

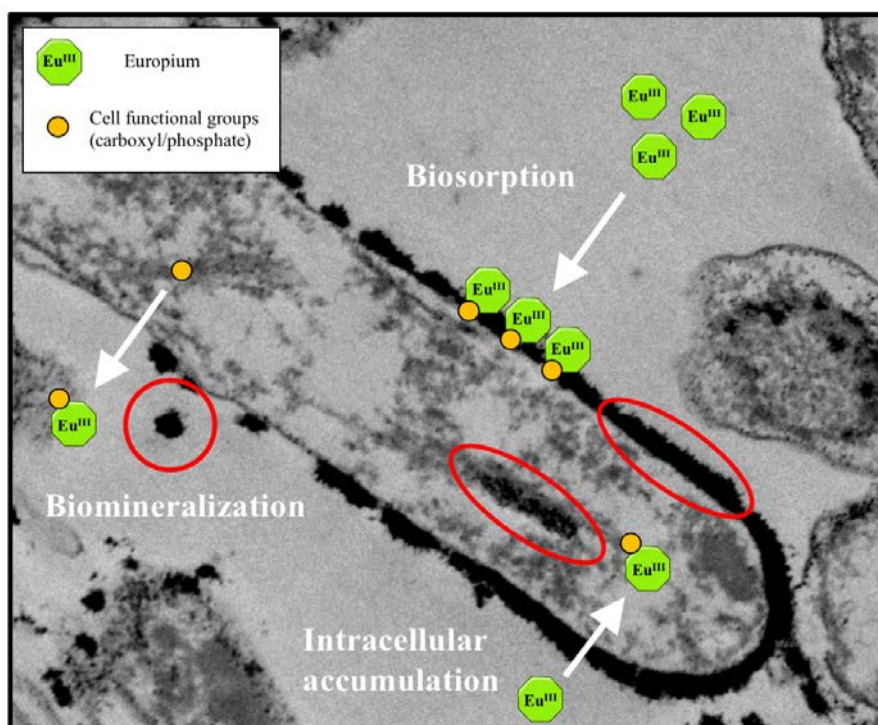
602 Table S1. Comparison of deprotonation constants and surface site concentrations for *S.*
603 *bentonitica* and other strains from different studies.

604 Table S2. Main infrared absorption bands of the bacterial cell functional groups

605 Table S3. Luminescence emission data of the Cm^{III}-*S. bentonitica* system including
606 those of relevant model systems for comparison.

607

608 **8. Table of content (TOC)/Abstract art**



609

610 **9. References**

- 611 (1) NEA. Radioactive Waste in Perspective. Paris, Nuclear Energy Agency. **2010**.
612 <https://doi.org/10.1787/9789264092624-en>.
- 613 (2) Stroes-Gascoyne, S.; Hamon, C. J.; Dixon, D. A.; Martino, J. B. Microbial Analysis of Samples from the
614 Tunnel Sealing Experiment at AECL's Underground Research Laboratory. *Phys. Chem. Earth* **2007**, *32* (1–
615 7), 219–231. <https://doi.org/10.1016/j.pce.2006.01.002>.
- 616 (3) Lopez-Fernandez, M.; Cherkouk, A.; Vilchez-Vargas, R.; Jauregui, R.; Pieper, D.; Boon, N.; Sanchez-
617 Castro, I.; Merroun, M. L. Bacterial Diversity in Bentonites, Engineered Barrier for Deep Geological
618 Disposal of Radioactive Wastes. *Microb. Ecol.* **2015**, *70* (4), 922–935. [https://doi.org/10.1007/s00248-015-0630-7](https://doi.org/10.1007/s00248-015-
619 0630-7).
- 620 (4) López-Fernández, M.; Fernández-Sanfrancisco, O.; Moreno-García, A.; Martín-Sánchez, I.; Sánchez-Castro,
621 I.; Merroun, M. L. Microbial Communities in Bentonite Formations and Their Interactions with Uranium.
622 *Appl. Geochemistry* **2014**, *49*, 77–86. <https://doi.org/10.1016/j.apgeochem.2014.06.022>.
- 623 (5) Meleshyn, A. Microbial Processes Relevant for Long-Term Performance of Radioactive Waste Repositories
624 in Clays. Gesellschaft für Anlagen-und Reaktorsicherheit (GRS) mbH. GRS – 291. **2011**. Available from:
625 <https://www.grs.de/sites/default/files/pdf/GRS-291.pdf>.
- 626 (6) Newsome, L.; Morris, K.; Lloyd, J. R. The Biogeochemistry and Bioremediation of Uranium and Other
627 Priority Radionuclides. *Chem. Geol.* **2014**, *363*, 164–184. <https://doi.org/10.1016/j.chemgeo.2013.10.034>.
- 628 (7) Gorietti, D.; Giardina, I.; Arginelli, D.; Battisti, P. Determination of Plutonium, Americium and Curium
629 Isotopes in Radioactive Metal Wastes Deriving from Nuclear Decommissioning. *J. Radioanal. Nucl. Chem.*
630 **2017**, *314* (3), 1785–1792. <https://doi.org/10.1007/s10967-017-5553-y>.
- 631 (8) Kooyman, T.; Buijron, L.; Rimpault, G. A Comparison of Curium, Neptunium and Americium
632 Transmutation Feasibility. *Ann. Nucl. Energy* **2018**, *112*, 748–758.
633 <https://doi.org/10.1016/j.anucene.2017.09.041>.
- 634 (9) Edelstein, N. M.; Klenze, R.; Fanghänel, T.; Hubert, S. Optical Properties of Cm(III) in Crystals and
635 Solutions and Their Application to Cm(III) Speciation. *Coord. Chem. Rev.* **2006**, *250* (7–8), 948–973.
636 <https://doi.org/10.1016/J.CCR.2006.02.004>.
- 637 (10) Ansoborlo, E.; Bion, L.; Doizi, D.; Moulin, C.; Lourenco, V.; Madic, C.; Cote, G.; Van der Lee, J.; Moulin,
638 V. Current and Future Radionuclide Speciation Studies in Biological Media. *Radiat. Prot. Dosimetry* **2007**,
639 *127* (1–4), 97–102. <https://doi.org/10.1093/rpd/ncm258>.
- 640 (11) Shukla, A.; Parmar, P.; Saraf, M. Radiation, Radionuclides and Bacteria: An in-Perspective Review. *J.
641 Environ. Radioact.* **2017**, *180* (11), 27–35. <https://doi.org/10.1016/j.jenvrad.2017.09.013>.
- 642 (12) Moll, H.; Lütke, L.; Bachvarova, V.; Cherkouk, A.; Selenska-Pobell, S.; Bernhard, G. Interactions of the
643 Mont Terri Opalinus Clay Isolate *Sporomusa* sp. MT-2.99 with Curium(III) and Europium(III).
644 *Geomicrobiol. J.* **2014**, *31* (8), 682–696. <https://doi.org/10.1080/01490451.2014.889975>.
- 645 (13) Reitz, T.; Rossberg, A.; Barkleit, A.; Steudtner, R.; Selenska-Pobell, S.; Merroun, M. L. Spectroscopic
646 Study on Uranyl Carboxylate Complexes Formed at the Surface Layer of *Sulfolobus acidocaldarius*. *Dalt.
647 Trans.* **2015**, *44* (6), 2684–2692. <https://doi.org/10.1039/c4dt02555e>.
- 648 (14) Moll, H.; Lütke, L.; Barkleit, A.; Bernhard, G. Curium(III) Speciation Studies with Cells of a Groundwater
649 Strain of *Pseudomonas fluorescens*. *Geomicrobiol. J.* **2013**, *30* (4), 337–346.
650 <https://doi.org/10.1080/01490451.2012.688927>.
- 651 (15) Lopez-Fernandez, M.; Moll, H.; Merroun, M. L. Reversible pH-Dependent Curium(III) Biosorption by the
652 Bentonite Yeast Isolate *Rhodotorula mucilaginosa* BII-R8. *J. Hazard. Mater.* **2018**, *370*, 156–163.
653 [https://doi.org/https://doi.org/10.1016/j.jhazmat.2018.06.054](https://doi.org/10.1016/j.jhazmat.2018.06.054).
- 654 (16) Bader, M.; Moll, H.; Steudtner, R.; Lösch, H.; Drobot, B.; Stumpf, T.; Cherkouk, A. Association of Eu(III)
655 and Cm(III) onto an Extremely Halophilic Archaeon. *Environ. Sci. Pollut. Res.* **2019**, *26* (9), 9352–9364.
656 <https://doi.org/10.1007/s11356-019-04165-7>.
- 657 (17) Ojeda, J. J.; Romero-González, M. E.; Bachmann, R. T.; Edyvean, R. G. J.; Banwart, S. A. Characterization
658 of the Cell Surface and Cell Wall Chemistry of Drinking Water Bacteria by Combining XPS, FTIR
659 Spectroscopy, Modeling, and Potentiometric Titrations. *Langmuir* **2008**, *24* (8), 4032–4040.

- 660 https://doi.org/10.1021/la702284b.
- 661 (18) Fein, J. B.; Boily, J. F.; Yee, N.; Gorman-Lewis, D.; Turner, B. F. Potentiometric Titrations of *Bacillus* 662 *Subtilis* Cells to Low PH and a Comparison of Modeling Approaches. *Geochim. Cosmochim. Acta* **2005**, *69* 663 (5), 1123–1132. https://doi.org/10.1016/j.gca.2004.07.033.
- 664 (19) Krawczyk-Bärsch, E.; Gerber, U.; Müller, K.; Moll, H.; Rossberg, A.; Steudtner, R.; Merroun, M. L. 665 Multidisciplinary Characterization of U(VI) Sequestration by *Acidovorax facilis* for Bioremediation 666 Purposes. *J. Hazard. Mater.* **2018**, *347*, 233–241. https://doi.org/10.1016/j.jhazmat.2017.12.030.
- 667 (20) Villar, M. V.; Pérez del Villar, L.; Martín, P. L.; Pelayo, M.; Fernández, A. M.; Garralón, A.; Cuevas, J.; 668 Leguey, S.; Caballero, E.; Huertas, F. J.; Jiménez de Cisneros, C.; Linares, J.; Reyes, E.; Delgado, A.; 669 Fernández-Soler, J. M.; Astudillo, J. The Study of Spanish Clays for Their Use as Sealing Materials in 670 Nuclear Waste Repositories: 20 Years of Progress. *J. Iber. Geol.* **2006**, *32* (1), 15–36.
- 671 (21) Ruiz Fresneda, M. A.; Delgado Martín, J.; Gómez Bolívar, J.; Fernández Cantos, M. V.; Bosch-Estevez, G.; 672 Martínez Moreno, M. F.; Merroun, M. L. Green Synthesis and Biotransformation of Amorphous Se 673 Nanospheres to Trigonal 1D Se Nanostructures: Impact on Se Mobility within the Concept of Radioactive 674 Waste Disposal. *Environ. Sci. Nano* **2018**, *5* (9), 2103–2116. https://doi.org/10.1039/c8en00221e.
- 675 (22) Sánchez-Castro, I.; Ruiz-Fresneda, M. A.; Bakkali, M.; Kämpfer, P.; Glaeser, S. P.; Busse, H. J.; López- 676 Fernández, M.; Martínez-Rodríguez, P.; Merroun, M. L. *Stenotrophomonas bentonitica* sp. nov., Isolated 677 from Bentonite Formations. *Int. J. Syst. Evol. Microbiol.* **2017**, *67* (8), 2779–2786. 678 https://doi.org/10.1099/ijsem.0.002016.
- 679 (23) Omoike, A.; Chorover, J. Spectroscopic Study of Extracellular Polymeric Substances from *Bacillus subtilis*: 680 Aqueous Chemistry and Adsorption Effects. *Biomacromolecules* **2004**, *5* (4), 1219–1230. 681 https://doi.org/10.1021/bm034461z.
- 682 (24) Fairley, N. CasaXPS 2.3.17 ed.; Casa Software Ltd. **2006**. Available from: www.casaxps.com
- 683 (25) Fein, J. B.; Daughney, C. J.; Yee, N.; Davis, T. A. A Chemical Equilibrium Model for Metal Adsorption 684 onto Bacterial Surfaces. *Geochim. Cosmochim. Acta* **1997**, *61* (16), 3319–3328. 685 https://doi.org/10.1016/S0016-7037(97)00166-X.
- 686 (26) Turner, B. F.; Fein, J. B. Prototif: A Program for Determining Surface Protonation Constants from Titration 687 Data. *Comput. Geosci.* **2006**, *32* (9), 1344–1356. https://doi.org/10.1016/j.cageo.2005.12.005.
- 688 (27) Borrok, D. M.; Fein, J. B. The Impact of Ionic Strength on the Adsorption of Protons, Pb, Cd, and Sr onto 689 the Surfaces of Gram Negative Bacteria: Testing Non-Electrostatic, Diffuse, and Triple-Layer Models. *J. 690 Colloid Interface Sci.* **2005**. https://doi.org/10.1016/j.jcis.2005.01.015.
- 691 (28) Borrok, D.; Turner, B. F.; Fein, J. B. A Universal Surface Complexation Framework for Modeling Proton 692 Binding onto Bacterial Surfaces in Geologic Settings. *Am. J. Sci.* **2005**. https://doi.org/10.2475/ajs.305.6- 693 8.826.
- 694 (29) Ngwenya, B. T.; Sutherland, I. W.; Kennedy, L. Comparison of the Acid-Base Behaviour and Metal 695 Adsorption Characteristics of a Gram-Negative Bacterium with Other Strains. *Appl. Geochemistry* **2003**, *18* 696 (4), 527–538. https://doi.org/10.1016/S0883-2927(02)00118-X.
- 697 (30) Dittrich, M.; Sibler, S. Cell Surface Groups of Two Picocyanobacteria Strains Studied by Zeta Potential 698 Investigations, Potentiometric Titration, and Infrared Spectroscopy. *J. Colloid Interface Sci.* **2005**, *286* (2), 699 487–495. https://doi.org/10.1016/j.jcis.2005.01.029.
- 700 (31) Yee, N.; Benning, L. G.; Phoenix, V. R.; Ferris, F. G. Characterization of Metal-Cyanobacteria Sorption 701 Reactions: A Combined Macroscopic and Infrared Spectroscopic Investigation. *Environ. Sci. Technol.* **2004**, 702 *38* (3), 775–782. https://doi.org/10.1021/es0346680.
- 703 (32) Yee, N.; Fein, J. Cd Adsorption onto Bacterial Surfaces: A Universal Adsorption Edge? *Geochim. 704 Cosmochim. Acta* **2001**, *65* (13), 2037–2042. https://doi.org/10.1016/S0016-7037(01)00587-7.
- 705 (33) Claessens, J.; van Lith, Y.; Laverman, A. M.; Van Cappellen, P. Acid-Base Activity of Live Bacteria: 706 Implications for Quantifying Cell Wall Charge. *Geochim. Cosmochim. Acta* **2006**, *70* (2), 267–276. 707 https://doi.org/10.1016/j.gca.2005.09.006.
- 708 (34) Merroun, M. L.; Nedelkova, M.; Ojeda, J. J.; Reitz, T.; Fernández, M. L.; Arias, J. M.; Romero-González, 709 M.; Selenska-Pobell, S. Bio-Precipitation of Uranium by Two Bacterial Isolates Recovered from Extreme 710 Environments as Estimated by Potentiometric Titration, TEM and X-Ray Absorption Spectroscopic

- 711 Analyses. *J. Hazard. Mater.* **2011**, *197*, 1–10. <https://doi.org/10.1016/j.hazmat.2011.09.049>.
- 712 (35) Fang, L.; Yang, S.; Huang, Q.; Xue, A.; Cai, P. Biosorption Mechanisms of Cu(II) by Extracellular
713 Polymeric Substances from *Bacillus subtilis*. *Chem. Geol.* **2014**, *386*, 143–151.
714 <https://doi.org/10.1016/j.chemgeo.2014.08.017>.
- 715 (36) Liu, Y.; Alessi, D. S.; Owtram, G. W.; Petrush, D. A.; Młoszewska, A. M.; Lalonde, S. V.; Martinez, R. E.;
716 Zhou, Q.; Konhauser, K. O. Cell Surface Reactivity of *Synechococcus* sp. PCC 7002: Implications for Metal
717 Sorption from Seawater. *Geochim. Cosmochim. Acta* **2015**, *169*, 30–44.
718 <https://doi.org/10.1016/j.gca.2015.07.033>.
- 719 (37) Ozaki, T.; Gillow, J. B.; Kimura, T.; Ohnuki, T.; Yoshida, Z.; Francis, A. J. Sorption Behavior of
720 Europium(III) and Curium(III) on the Cell Surfaces of Microorganisms. In *Radiochimica Acta*; **2004**, *92* (9–
721 11), 741–748. <https://doi.org/10.1524/ract.92.9.741.55006>.
- 722 (38) Yao, T.; Wu, X.; Chen, X.; Xiao, Y.; Zhang, Y.; Zhao, Y.; Li, F. Biosorption of Eu(III) and U(VI) on
723 *Bacillus subtilis*: Macroscopic and Modeling Investigation. *J. Mol. Liq.* **2016**, *219*, 32–38.
724 <https://doi.org/10.1016/j.molliq.2016.01.101>.
- 725 (39) Gadd, G. M. Biosorption: Critical Review of Scientific Rationale, Environmental Importance and
726 Significance for Pollution Treatment. *J. Chem. Technol. Biotechnol.* **2009**, *84* (1), 13–28.
727 <https://doi.org/10.1002/jctb.1999>.
- 728 (40) Jiang, W.; Saxena, A.; Song, B.; Ward, B. B.; Beveridge, T. J.; Myneni, S. C. B. Elucidation of Functional
729 Groups on Gram-Positive and Gram-Negative Bacterial Surfaces Using Infrared Spectroscopy. *Langmuir*
730 **2004**, *20* (26), 11433–11442. <https://doi.org/10.1021/la049043+>.
- 731 (41) Chu, H. A.; Hillier, W.; Debus, R. J. Evidence That the C-Terminus of the D1 Polypeptide of Photosystem II
732 Is Ligated to the Manganese Ion That Undergoes Oxidation during the S1 to S2 Transition: An Isotope-
733 Edited FTIR Study. *Biochemistry* **2004**, *43* (11), 3152–3166. <https://doi.org/10.1021/bi035915f>.
- 734 (42) Nakamoto, K. Infrared and Raman Spectra of Inorganic and Coordination Compounds: Part B: Applications
735 in Coordination, Organometallic, and Bioinorganic Chemistry, Sixth Edit.; **2008**.
736 <https://doi.org/10.1002/9780470405888>.
- 737 (43) Tackett, J. E. FT-IR Characterization of Metal Acetates in Aqueous Solution. *Appl. Spectrosc.* **1989**, *43* (3),
738 483–489. <https://doi.org/10.1366/0003702894202931>.
- 739 (44) Deacon, G. B.; Phillips, R. J. Relationships between the Carbon-Oxygen Stretching Frequencies of
740 Carboxylato Complexes and the Type of Carboxylate Coordination. *Coord. Chem. Rev.* **1980**, *33* (3), 227–
741 250. [https://doi.org/10.1016/S0010-8545\(00\)80455-5](https://doi.org/10.1016/S0010-8545(00)80455-5).
- 742 (45) Kumar, S.; Prakash, R.; Singh, V. Synthesis, Characterization, and Applications of Europium Oxide: A
743 Review. *Rev. Adv. Sci. Eng.* **2015**, *4* (4), 247–257. <https://doi.org/10.1166/rase.2015.1102>.
- 744 (46) Pradier, C. M.; Rubio, C.; Poleunis, C.; Bertrand, P.; Marcus, P.; Compère, C. Surface Characterization of
745 Three Marine Bacterial Strains by Fourier Transform IR, X-Ray Photoelectron Spectroscopy, and Time-of-
746 Flight Secondary-Ion Mass Spectrometry, Correlation with Adhesion on Stainless Steel Surfaces. *J. Phys.
747 Chem. B.* **2005**, *109* (19), 9540–9549. <https://doi.org/10.1021/jp044705p>.
- 748 (47) Van Der Mei, H. C.; De Vries, J.; Busscher, H. J. X-Ray Photoelectron Spectroscopy for the Study of
749 Microbial Cell Surfaces. *Surf. Sci. Rep.* **2000**, *39* (1), 1–24. [https://doi.org/10.1016/S0167-5729\(00\)00003-0](https://doi.org/10.1016/S0167-5729(00)00003-0).
- 750 (48) Dufrêne, Y. F.; Van der Wal, A.; Norde, W.; Rouxhet, P. G. X-Ray Photoelectron Spectroscopy Analysis of
751 Whole Cells and Isolated Cell Walls of Gram-Positive Bacteria: Comparison with Biochemical Analysis. *J.
752 Bacteriol.* **1997**, *179* (4), 1023–1028. <https://doi.org/10.1128/jb.179.4.1023-1028.1997>.
- 753 (49) Dufrêne, Y. F.; Rouxhet, P. G. X-Ray Photoelectron Spectroscopy Analysis of the Surface Composition of
754 *Azospirillum brasilense* in Relation to Growth Conditions. *Colloids Surfaces B Biointerfaces* **1996**, *7* (5–6),
755 271–279. [https://doi.org/10.1016/0927-7765\(96\)01295-7](https://doi.org/10.1016/0927-7765(96)01295-7).
- 756 (50) Mercier, F.; Alliot, C.; Bion, L.; Thromat, N.; Toulhoat, P. XPS Study of Eu(III) Coordination Compounds:
757 Core Levels Binding Energies in Solid Mixed-Oxo-Compounds Eum_xO_y. *J. Electron Spectros. Relat.
758 Phenomena* **2006**, *150* (1), 21–26. <https://doi.org/10.1016/j.elspec.2005.08.003>.
- 759 (51) Merroun, M. L.; Raff, J.; Rossberg, A.; Hennig, C.; Reich, T.; Selenska-Pobell, S. Complexation of Uranium
760 by Cells and S-Layer Sheets of *Bacillus sphaericus* JG-A12. *Appl. Environ. Microbiol.* **2005**, *71* (9), 5532–
761 5543. <https://doi.org/10.1128/AEM.71.9.5532-5543.2005>.

- 762 (52) Fahmy, K.; Merroun, M.; Pollmann, K.; Raff, J.; Savchuk, O.; Hennig, C.; Selenska-Pobell, S. Secondary
763 Structure and Pd(II) Coordination in S-Layer Proteins from *Bacillus sphaericus* Studied by Infrared and X-
764 Ray Absorption Spectroscopy. *Biophys. J.* **2006**, *91* (3), 996-1007.
765 https://doi.org/10.1529/biophysj.105.079137.
- 766 (53) Texier, A. C.; Andrés, Y.; Illemassene, M.; Le Cloirec, P. Characterization of Lanthanide Ions Binding Sites
767 in the Cell Wall of *Pseudomonas aeruginosa*. *Environ. Sci. Technol.* **2000**, *34* (4), 610–615.
768 https://doi.org/10.1021/es990668h.
- 769 (54) Markai, S.; Andrès, Y.; Montavon, G.; Grambow, B. Study of the Interaction between Europium (III) and
770 *Bacillus subtilis*: Fixation Sites, Biosorption Modeling and Reversibility. *J. Colloid Interface Sci.* **2003**, *262*
771 (2), 351–361. https://doi.org/10.1016/S0021-9797(03)00096-1.
- 772 (55) Toyofuku, M.; Nomura, N.; Eberl, L. Types and Origins of Bacterial Membrane Vesicles. *Nat. Rev. Microbiol.* **2019**, *17*, 13-24. https://doi.org/10.1038/s41579-018-0112-2.
- 774 (56) Jan, A. T. Outer Membrane Vesicles (OMVs) of Gram-Negative Bacteria: A Perspective Update. *Front. Microbiol.* **2017**, *8*, 1053. https://doi.org/10.3389/fmicb.2017.01053.
- 776 (57) Klimentová, J.; Stulík, J. Methods of Isolation and Purification of Outer Membrane Vesicles from Gram-
777 Negative Bacteria. *Microbiol. Res.* **2015**, *170*, 1-9. https://doi.org/10.1016/j.micres.2014.09.006.
- 778 (58) Gadd, G. M. Microbial Influence on Metal Mobility and Application for Bioremediation. In *Geoderma*;
779 **2004**, *122* (2-4), 109-119. https://doi.org/10.1016/j.geoderma.2004.01.002.
- 780 (59) Niba, E. T. E.; Naka, Y.; Nagase, M.; Mori, H.; Kitakawa, M. A Genome-Wide Approach to Identify the
781 Genes Involved in Biofilm Formation in *E. coli*. *DNA Res.* **2007**, *14* (6), 237–246.
782 https://doi.org/10.1093/dnarese/dsm024.
- 783 (60) Prigent-Combaret, C.; Vidal, O.; Dorel, C.; Lejeune, P. Abiotic Surface Sensing and Biofilm-Dependent
784 Regulation of Gene Expression in Escherichia Coli. *J. Bacteriol.* **1999**, *181* (19), 5993-6002.
- 785 (61) Sánchez-Castro, I.; Bakkali, M.; Merroun, M. L. Draft Genome Sequence of *Stenotrophomonas bentonitica*
786 BII-R7, a Selenite-Reducing Bacterium Isolated from Spanish Bentonites. *Genome Announc.* **2017**, *5* (31).
787 https://doi.org/10.1128/genomeA.00719-17.
- 788 (62) Clark, M. E.; Edelmann, R. E.; Duley, M. L.; Wall, J. D.; Fields, M. W. Biofilm Formation in *Desulfovibrio*
789 *vulgaris* Hildenborough Is Dependent upon Protein Filaments. *Environ. Microbiol.* **2007**, *9* (11).
790 https://doi.org/10.1111/j.1462-2920.2007.01398.x.
- 791 (63) Rui, X.; Kwon, M. J.; O'Loughlin, E. J.; Dunham-Cheatham, S.; Fein, J. B.; Bunker, B.; Kemner, K. M.;
792 Boyanova, M. I. Bioreduction of Hydrogen Uranyl Phosphate: Mechanisms and U(IV) Products. *Environ. Sci. Technol.* **2013**, *47* (11), 5668–5678. https://doi.org/10.1021/es305258p.

794